

The Impact of Nova Outbursts on the Chemical Abundance of the Interstellar Medium

Guoli He¹, Chunhua Zhu¹, Guoliang Lü^{2,1}, Lin Li¹, Sufen Guo¹, Helei Liu¹, and Jun Gao¹
School of Physical Science and Technology, Xinjiang University, Urumqi 830017, China; chunhuazhu@sina.cn, guolianglv@xao.ac.cn
² Xinjiang Astronomical Observatory, Chinese Academy of Sciences, Urumqi 830011, China
Received 2024 May 15; revised 2024 August 14; accepted 2024 August 20; published 2024 October 4

Abstract

Nova outbursts are the results of thermonuclear runaways, which occur when sufficient material accretes on the surfaces of white dwarfs (WDs). Using the MESA code, we construct a detailed grid for carbon-oxygen and oxygen-neon-magnesium novae. By employing population synthesis methods, we conduct a statistical analysis of the distribution of novae in the Milky Way. In our models, on average, a typical nova system may undergo about 8000 eruptions and the Galactic nova rate is $\sim 130\,\mathrm{yr}^{-1}$. The C, N, and O elements in nova ejecta are strongly affected by the mixing degree between WD core and accreted material. Our results show that the average value of $^{12}\mathrm{C}/^{13}\mathrm{C}$ in nova ejecta is about an order of magnitude lower than that on the surface of a red giant, that for $^{16}\mathrm{O}/^{17}\mathrm{O}$ is about 5 times lower, and that for $^{14}\mathrm{N}/^{15}\mathrm{N}$ is about 1.5 times lower. The annual yields of $^{13}\mathrm{C}$, $^{15}\mathrm{N}$, and $^{17}\mathrm{O}$ from nova ejection are larger than those from AGB stars. This indicates that compared to a red giant, nova eruptions are a more important source of the odd-numbered nuclear elements of $^{13}\mathrm{C}$, $^{15}\mathrm{N}$, and $^{17}\mathrm{O}$ in the Galactic interstellar medium.

Key words: ISM: abundances – (stars:) novae – cataclysmic variables – (stars:) white dwarfs

1. Introduction

Big Bang nucleosynthesis provided hydrogen (H), helium (He), and trace amounts of lithium in the early universe, while other elements have been mainly produced in some types of stars: low-mass stars by stellar wind, massive stars by supernova ejecta, binary systems by the ejecta triggered via common envelope evolution (CEE) or binary mergers (Kennedy 2011). Usually, based on a low mass ejected $(10^{-5}M_{\odot})$ by nova outbursts, novae are considered a negligible origin of the elements. Gehrz et al. (1998) estimated that about 0.3% of the interstellar medium (ISM) is produced by nova outbursts.

However, some high-resolution spectra of novae have revealed that the ejected material is highly enriched in metals (e. g., Livio & Truran 1994; Gehrz et al. 1998). More importantly, observational evidences indicate that the oddnumbered nuclei of ¹³C in nova outbursts significantly differ from those of the Sun (Evans et al. 1988; Pavlenko et al. 2010). Based on a high resolution infrared spectrum, Pavlenko et al. (2004) found that $^{12}\text{C}/^{13}\text{C}$ of V4334 Sgr is about 4 ± 1 , which is far higher than that of the Sun. Many theoretical calculations have estimated that the odd-numbered nuclei ¹³C, ¹⁵N, and ¹⁷O in the Galaxy may mainly originate from nova outbursts (e. g., Starrfield et al. 1972, 1997; Kovetz & Prialnik 1997; José & Hernanz 1998, 2007; Li et al. 2016; Das 2021), and they also considered that novae may also contribute to other nuclei, such as ⁷Li, ²²Na and ²⁶Al (José et al. 1997; Hernanz 2012; Bennett et al. 2013; Gao et al. 2024).

In fact, there are many theoretical literatures for simulating nova outbursts (Starrfield et al. 1972; Prialnik 1986; Denissenkov et al. 2013). They calculated thermonuclear runaway (TNR) and element abundances of nova outbursts. Applying the method of population synthesis, Li et al. (2016) calculated the contribution of chemical abundances in nova ejecta to the ISM. In their work, based on the 26 models proposed by Yaron et al. (2005) and the 10 models proposed by Kovetz & Prialnik (1997), bilinear interpolation was performed, but their results hardly cover all observations (see Figures 1-3 in Li et al. 2016). The main reasons are as follows: First, the fitting formula for calculating chemical abundances cannot reflect the changes produced by different mass-accretion rates. Second, there are very large observational errors in measuring the chemical abundance ratios of novae. For example, the C abundance in nova PW Vul ejecta measured by Hassall et al. (1990) (0.032) is about an order of magnitude higher than that in Saizar et al. (1991) (0.0033). Chen et al. (2016) and Chen et al. (2019) investigated nova populations, and published the comprehensive nova models. However, they did not discuss the element contribution of nova ejecta to the Milky Way.

In this paper, we construct a complete grid for nova outbursts, and estimate the contribution of various chemical elements to the Milky Way. In Section 2, the simulation method and the main input parameters are introduced. In Section 3, we show the element yields produced by nova outbursts. A summary is given in Section 4.

2. Models

In order to investigate the impact of nova outbursts on the chemical abundance of the Galactic ISM, we use Modules for Experiments in Stellar Astrophysics (MESA; Paxton et al. 2011, 2013, 2015, [rev. 12778]) to simulate the TNRs, and apply the rapid binary evolution code Binary Star Evolution (BSE, Hurley et al. 2002) and population synthesis to estimate the element yields of nova populations.

2.1. Nova Outburst

The nova module in MESA has been widely used (Denissenkov et al. 2013; Guo et al. 2022; Shen & Quataert 2022). In the model of nova outburst, the main factors influencing the timing and intensity of TNRs are the white dwarf (WD) mass $(M_{\rm WD})$, mass accretion rate (\dot{M}) , core temperature of the WD (T_C) , and chemical composition of the accreted material (Shara et al. 1986; Livio et al. 1988; Yaron et al. 2005). In this paper, we select CO WDs with masses of $0.6 M_{\odot}$, $0.7 M_{\odot}$, $0.8 M_{\odot}$, $0.9 M_{\odot}$, $1.0 M_{\odot}$, $1.1 M_{\odot}$, and ONeMg WDs with masses of $1.1 M_{\odot}$, $1.2 M_{\odot}$, $1.3 M_{\odot}$. The mass ranges overlap because the boundary between CO and ONeMg novae cannot be precisely determined at present. The $T_{\rm C}$ is assumed to be 3×10^7 K. In simulations of nova eruptions, the selection of $T_{\rm C}$ is generally within the range of $1 \times 10^7 \, {\rm K}$ to $5 \times 10^7 \, {\rm K}$. Schwartzman et al. (1994) investigated the influence of $T_{\rm C}$ on nova eruptions and demonstrated that it affects the evolution of the nova eruption through two mechanisms: in cold WDs heat conduction into the core delays the ignition of hydrogen, and thus results in relatively long accretion times (large accreted masses); hot WDs have an outer convective layer that enhances the mixing process between the accreted hydrogen-rich material and heavy elements of the core, thus hastening the occurrence of the TNR. Yaron et al. (2005) indicated the WD mass restriction is weaker for lower temperatures. Chen et al. (2016) investigated the influence of different $T_{\rm C}$ on the nova rate and found no significant differences. The nova rate for higher $T_{\rm C}$ was only slightly higher than that for lower $T_{\rm C}$. Shara et al. (2018) mentioned that compared to other influencing factors, the $T_{\rm C}$ has a much smaller impact on the results. Therefore, we choose an intermediate value of 3×10^7 K, in order to limit the parameter space. We have adopted mass accretion rates of $1.0\times10^{-11}\,M_\odot\,\mathrm{yr}^{-1},\ 1.0\times10^{-10}\,M_\odot\,\mathrm{yr}^{-1},\ 1.0\times10^{-9}\,M_\odot\,\mathrm{yr}^{-1},$ and $1.0\times10^{-8}\,M_\odot\,\mathrm{yr}^{-1}.$

Based on the enrichment of CNO or ONeMg abundances in the nova models, in order to better match the abundance determination results from spectroscopy, it is assumed that the transferred material from the companion star is solar-like and mixed with the outermost layers of the underlying core through an unknown mechanism (shear mixing, diffusion, or a convective multi-dimensional process) with a given fraction (Politano et al. 1995; José et al. 1997; Guo et al. 2022). The degree of mixing can be modified by artificially assigning different abundances to the

accreted material. In our simulations, the solar chemical composition data are taken from Lodders & Palme (2009). Following José & Hernanz (1998), initial chemical abundances for CO cores are $X(^{12}\text{C}) = 0.495$, $X(^{16}\text{O}) = 0.495$, and $X(^{22}\text{Ne}) = 0.01$. For the ONeMg cores, the chemical composition is assumed to be $X(^{12}\text{C}) = 0.00916$, $X(^{16}\text{O}) = 0.511$, $X(^{20}\text{Ne}) = 0.313$, $X(^{21}\text{Ne}) = 0.00598$, $X(^{22}\text{Ne}) = 0.00431$, $X(^{23}\text{Na}) = 0.0644$, $X(^{24}\text{Mg}) = 0.0548$, $X(^{25}\text{Mg}) = 0.0158$, $X(^{26}\text{Mg}) = 0.00989$, and $X(^{27}\text{Al}) = 0.0108$ (Ritossa et al. 1996).

In addition, the mixing degree between WD core and envelope greatly affects the TNR (Starrfield et al. 1997, 2020; Hillman et al. 2014). According to the mixing model proposed by Politano et al. (1995), the transferred material from the companion star is assumed to be a mixture of solar-like matter and the outermost shells of the underlying WD. In our model, we consider different WD mixing fractions $f_{\rm WD} = 25\%$, 50%, and 75%.

2.2. Method of Population Synthesis

In order to evolve the nova populations, we apply the method of population synthesis which has been used by our group (e. g., Lü et al. 2008, 2013; Gao et al. 2022; Zhu et al. 2023). Following this literature, the initial mass function of Miller & Scalo (1979) and a flat distribution of mass ratios (Eggleton et al. 1989) are used. The binary separations are distributed by $\log a = 5X + 1$, where a is the separation in R_{\odot} . Here, X is a uniformly random variable in the range [0, 1].

Through the method of population synthesis, we create 10⁶ binary systems, and we use BSE code to evolve these binaries for nova populations. The formation of nova systems usually involves CEE (Han et al. 2020; Chen et al. 2024). In BSE, a binary undergoing CEE is determined by the critical mass ratio $q_{\rm c}$. If $q = M_{\rm donor}/M_{\rm gainer}$ is larger than $q_{\rm c}$, the binary system undergoes CEE when the donor fills its Roche lobe. Based on the adiabatic mass-loss model, Ge et al. (2010, 2015) and Ge et al. (2020) calculated q_c and constructed a grid for q_c . In this work, we use q_c in Ge et al. (2020). During CEE, the binary system undergoes a dynamical spiral-in which depends on the combined parameter $\alpha_{CE}\lambda$, where α_{CE} is the efficiency of the orbital energy used to expel the envelope of the donor, and λ parameterizes the envelope structure of the donor. Chen et al. (2016) discussed the effects of the parameter $\alpha_{\rm CE}\lambda$ on the nova populations. Here, we take $\alpha_{\rm CE}\lambda = 0.5$.

3. Results

Using MESA and BSE codes, we construct a detailed grid for nova outbursts and obtain a large sample for nova binary systems by the population synthesis method, respectively. Via the bilinear interpolation of WD mass and mass-accretion rate in the grid, the properties of all the nova populations can be depicted.

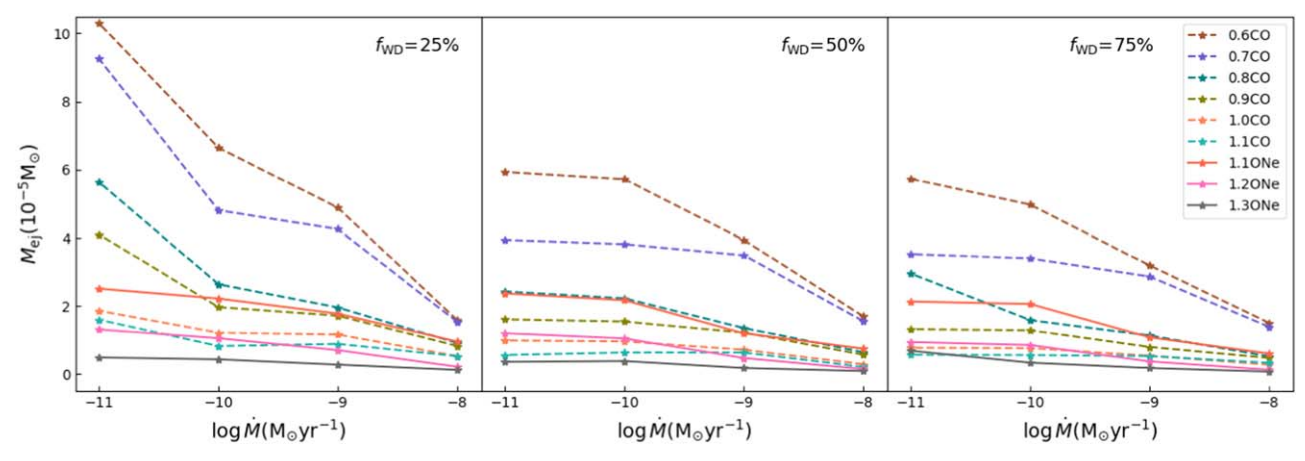


Figure 1. The ejecta mass from a nova outburst with different WD masses, mass-accretion rates and mixing degrees. The left, middle and right panels present the models with $f_{WD} = 25\%$, 50% and 75%, respectively. Dashed lines of various colors represent WDs with different masses noted in the upper-right region of the right panel.

3.1. Yields of Nova Outbursts

According to different WD masses, the mass-accretion rates and the mixing degrees, we simulate 108 models for nova outbursts, including 72 models for CO WDs and 36 models for ONeMg WDs. Theoretical simulations for nova outbursts have been nicely described by the previous investigations (e.g., Yaron et al. 2005; Chen et al. 2016). This work focuses on the element yields ejected by nova outbursts into the ISM.

During nova outbursts, the mass-loss rate from an accreting WD is calculated via

$$\dot{M} = -2 \frac{L - L_{\rm Edd}}{v_{\rm esc}},\tag{1}$$

where $v_{\rm esc}$ is the escape velocity at the photosphere of the WD, L is the luminosity of the outburst, and $L_{\rm Edd}$ is the Eddington luminosity. Here, $L_{\rm Edd} = \frac{4\pi {\rm c} M_{\rm WD}}{\kappa}$, where κ is the mass-weighted-mean Rosseland opacity of the outer layers of the WD. Therefore, the ejecta mass by a nova outburst can be estimated by

$$M_{\rm ej} = \int_{t_{\rm Edd}}^{t_0} \dot{M} dt, \tag{2}$$

where t_0 and $t_{\rm Edd}$ are the time of the beginning of the nova outburst and that when the luminosity is lower than $L_{\rm Edd}$, respectively.

Figure 1 shows the ejecta mass from a nova outburst including CO WD nova outbursts and ONe WD nova outbursts with different input parameters. For models with the same $f_{\rm WD}$ and \dot{M} , simulation results indicate that lower-mass WDs exhibit higher mass ejections. This is because as the mass of the WD increases, its radius decreases, but its gravitational potential increases (Chandrasekhar 1931, 1935). Consequently, during the accretion phase, a higher-mass WD has less critical ignition mass. The stronger gravitational potential imposes a tighter

constraint on the ejection process during a nova, leading to lower mass ejecta. For models with the same $f_{\rm WD}$ and $M_{\rm WD}$, the lower \dot{M} is, the larger the ejected mass is. This is because as the value of the \dot{M} increases, the temperature rises faster (Chomiuk et al. 2021), which results in less critical ignition mass and less ejected material. For models with the same $M_{\rm WD}$ and \dot{M} , the smaller the mixing degree is, the greater the ejected mass is. The main reason is that the increase of the mixing degree results in the increase of the opacity in the nuclear burning region, which leads to lower critical ignition mass and less ejected mass.

Theoretically, the range of ejecta mass from a nova outburst is between $\sim 10^{-7}$ and $10^{-4}\,M_\odot$ (Yaron et al. 2005; Chen et al. 2019). Observationally, the average ejecta mass for the known novae is $\sim 2\times 10^{-5}\,M_\odot$ (José & Hernanz 1998). Our results are consistent with observations.

We also compute the yields of some isotopes in nova ejecta. These isotopes include ¹H, ⁴He, ¹²C, ¹³C, ¹⁴N, ¹⁵N, ¹⁶O, ¹⁷O, ²⁰Ne and ²²Ne. We neglect the abundances of other isotopes because their chemical abundances are significantly smaller. The yields of these isotopes in different models are listed in Tables A1 and A2 of Appendix.

Kovetz & Prialnik (1997) simulated a CO nova eruption and provided chemical yield grids of five models. The abundances of 13 C, 15 N, and 17 O during a nova outburst in their models are $\sim 7.82 \times 10^{-3}$ – 9.14×10^{-4} , $\sim 1.89 \times 10^{-4}$ – 4.26×10^{-6} and $\sim 7.97 \times 10^{-3}$ – 5.47×10^{-4} respectively. Under similar input parameters, our results shown by Table 1 (Appendix) are higher than those calculated by Kovetz & Prialnik (1997). José & Hernanz (1998) gave the chemical yields of 12 nova models. The abundances of 13 C, 15 N, and 17 O during a nova outburst in their models are $\sim 1.3 \times 10^{-1}$ – 2.3×10^{-2} , $\sim 1.7 \times 10^{-2}$ – 9.3×10^{-4} and $\sim 4.1 \times 10^{-2}$ – 3.3×10^{-3} respectively. Under similar input parameters, our results are lower than those of José & Hernanz (1998) within a factor of ~ 8 . The main reasons are the different

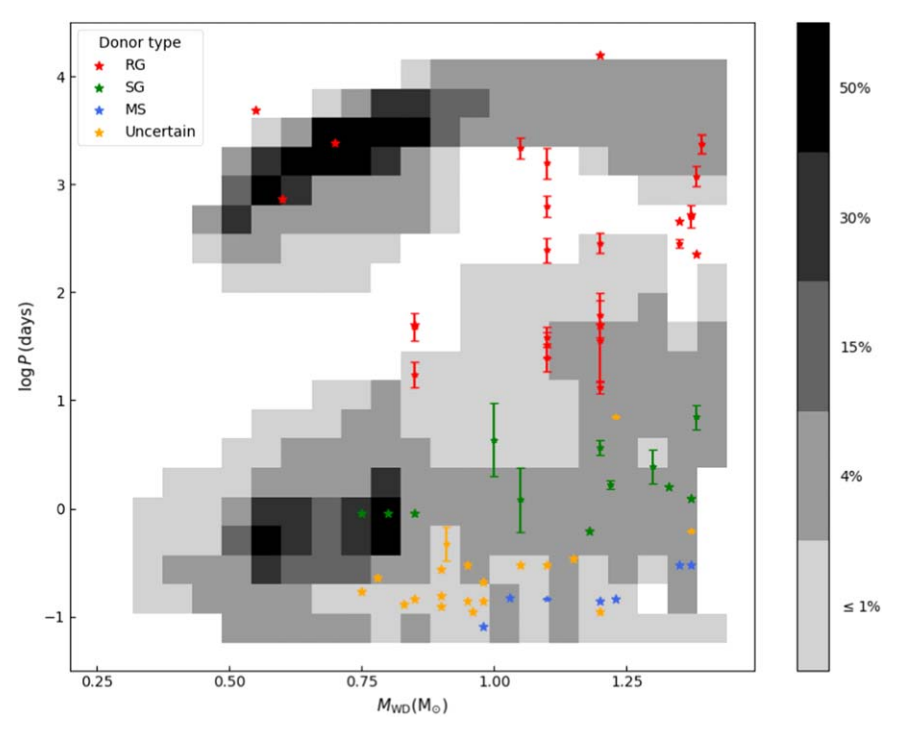


Figure 2. A gray distribution for the orbital periods and WD masses of the nova populations. The different colored stars represent observed nova systems. The red stars signify that WD companions are RG stars, the green stars are for subgiant stars, the blue stars are for MS stars, while the yellow stars are for uncertain type. The observed data come from Shara et al. (2018), Hachisu & Kato (2019), Schaefer (2022).

Ejecta Composition		Ejecta Mass $(M_{\odot} \text{ yr}^{-1})$			
•	CO Novae	ONeMg Novae	All Novae		
¹ H	6.1×10^{-4}	8.4×10^{-5}	7.0×10^{-4}		
⁴ He	2.7×10^{-4}	4.5×10^{-4}	3.1×10^{-4}		
¹² C	3.1×10^{-5}	1.5×10^{-6}	3.3×10^{-5}		
¹³ C	7.7×10^{-5}	2.7×10^{-6}	8.0×10^{-5}		
^{14}N	1.0×10^{-4}	7.2×10^{-6}	1.1×10^{-4}		
¹⁵ N	2.6×10^{-8}	4.7×10^{-6}	4.8×10^{-6}		
¹⁶ O	1.3×10^{-4}	2.5×10^{-5}	1.6×10^{-4}		
¹⁷ O	8.7×10^{-7}	1.9×10^{-6}	4.3×10^{-6}		
²⁰ Ne	1.1×10^{-6}	1.9×10^{-5}	2.0×10^{-5}		
²² Ne	1.9×10^{-6}	1.6×10^{-7}	2.1×10^{-6}		

nuclear yield grids selected and the different assumptions for the chemical composition of the CO and ONeMg cores. Additionally, the choice of different evolution codes also affects the results.

3.2. Contribution of Nova Populations to the ISM

Using BSE code and population synthesis, we create and evolve 10⁶ binary systems. About 2.5% of binary systems can evolve into nova systems. Figure 2 shows the distribution of orbital periods versus WD masses for these nova populations.

The nova populations in our model are divided into two subpopulations. The nova populations with orbital periods shorter than \sim 100 days have undergone CEE during WD formation, while most of ones with orbital periods wider than ~ 100 days have experienced stable mass transfer. In the former, WD companions may be main sequence (MS) stars or red giants (RGs), and mass transfer occurs via Roche lobe overflow. In the latter, WD companions are RGs, and WDs usually accrete matter via stellar winds. Compared to the observed nova populations, our result can basically cover observations. Based on Figure 2, we find that the WD's mass of nova systems ranges from $0.3 M_{\odot}$ to $1.38 M_{\odot}$, with a peak around $0.6 M_{\odot}$, which is consistent with the mass distribution of single WDs (Han et al. 1995). In observations, WD masses in novae are found $>0.55M_{\odot} \sim 0.6M_{\odot}$ (e. g., Horne et al. 1993; Smith et al. 1998; Thoroughgood et al. 2001; Kato & Hachisu 2011; Hachisu & Kato 2015; Selvelli & Gilmozzi 2019). Kato & Hachisu (2009) studied the condition of occurrence of optically thick winds. The border of WD mass for occurrence of winds lies at $M_{\rm WD,cr} \approx 0.6 M_{\odot} \sim 0.7 M_{\odot}$, depending on the metallicity. A shell flash on a WD $(M_{\rm WD} < M_{\rm WD,cr})$ evolves too slowly to be recognized as a nova outburst on a human timescale. Therefore, in order to better compare with observations, we select the lowest WD mass to be $0.6 M_{\odot}$ for the model grid in this work. Our simulation results align well with the observed data. However, the distribution of observed data is more concentrated in the

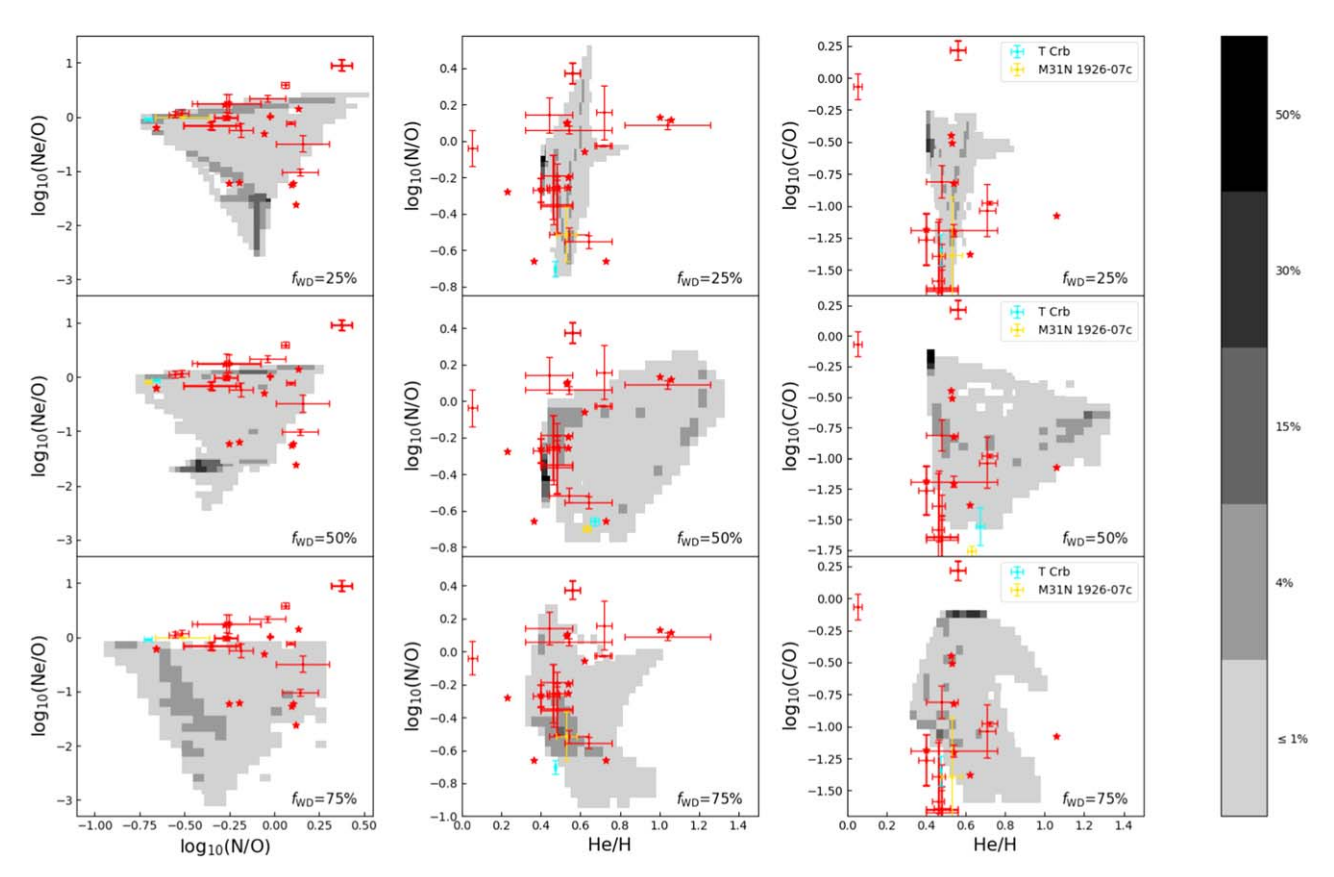


Figure 3. The abundance ratios of chemical elements in nova ejecta. Considering that the number of CO novae is 35 times that of ONeMg novae, we separate and normalize the CO novae and the ONeMg novae. In the left panel, the distribution of log(Ne/O) vs. log(N/O) is shown. The middle panel displays log(N/O) vs. He/H. The right panel depicts log(C/O) vs. He/H. Each row of images represents a different mixing level: 25% in the top row, 50% in the middle row, and 75% in the bottom row. The red pentagrams in the figures represent observational values from Lyke et al. (2003), Shore et al. (2003), Vanlandingham et al. (2005), Iijima (2006), Schwarz et al. (2007a, 2007b), Downen et al. (2013), Tylenda et al. (2019), while the blue and yellow dots give the predicted abundance ratio of the ejecta from novae T Crb and M31N 1926-07c. Their nova outbursts may occur in 2024 and 2025, respectively.

massive WD region, which differs from our mass distribution. Schreiber et al. (2016) proposed consequential angular momentum loss to solve the problem about the average WD mass in the observed nova systems higher than those of single WDs. However, the physical mechanism of consequential angular momentum loss is still unclear. Furthermore, the observational selection effect is also one of the reasons. The main reason is that massive WDs require less accreted material compared to lower-mass WDs to trigger TNR. Additionally, massive WDs exhibit more violent eruptions and have shorter recurrence timescales. The shorter the outburst period is, the higher the likelihood of being discovered as a nova. Therefore, although lower-mass WDs are more abundant in the Milky Way, the observed nova systems tend to have massive WDs.

3.3. CNO and Their Isotopes in Nova Ejecta

The nova populations created by BSE code can give the WD mass and the mass-accretion rate for every nova binary. By a

bilinear interpolation of the WD mass and the mass-accretion rate in the nova grid constructed via MESA code, we can give the chemical contribution of all the nova populations.

Figure 3 displays the abundance ratios of C, N, O, and Ne in the nova ejecta for $f_{WD} = 25\%$, 50%, and 75%. The left three panels in Figure 3 show the distribution of log(Ne/O) versus log(N/O) for nova populations. There are two peaks for log (Ne/O) distributions in the model with $f_{WD} = 25\%$ and 50%. The upper peak $(\log(Ne/O) \sim 0)$ represents the ejecta produced by ONeMg WD novae, while the bottom peak (log $(Ne/O) \sim -2)$ originates from CO WD novae. When f_{WD} increases up to 75%, our results cannot cover the novae with $\log(\text{Ne/O})$ higher than 0. As the f_{WD} increases, the abundance of Ne and O elements in the accreted material increases. Since classical nova outbursts on CO WDs achieve lower peak temperatures than those exploding on ONe cores, and also because of the lack of significant amounts of "seed" NeNa-MgAl nuclei in CO WDs, CO novae show prominent nuclear activity in the CNO region. In contrast, ONeMg novae exhibit

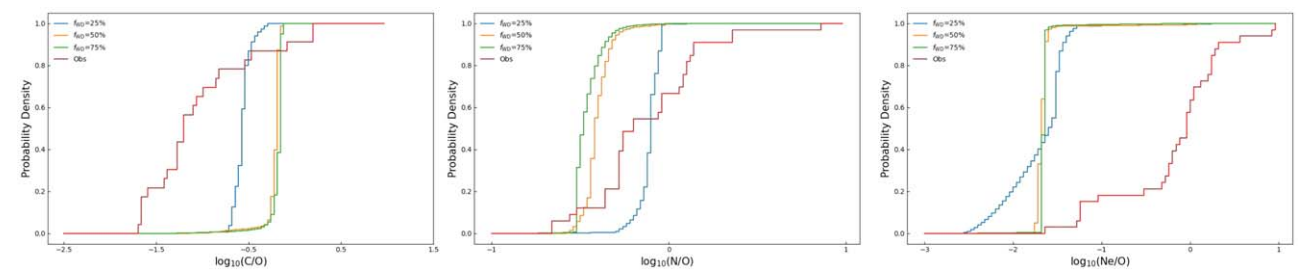


Figure 4. K–S test for the models with $f_{WD} = 25\%$, 50%, 75% and observational values. The left, middle and right panels present the models with $\log(C/O)$, $\log(N/O)$ and $\log(Ne/O)$, respectively.

greater nuclear activity, and current predictions suggest that it may extend up to Ca (José et al. 2006). In the left panels, CO novae are concentrated in the lower part. During the outburst phase, the O elements are converted into heavier elements, while the Ne elements are not significantly affected. Therefore, as $f_{\rm WD}$ increases to 75%, $\log({\rm Ne/O})$ decreases. The middle three panels in Figure 3 show the distribution of log(N/O)versus He/H for nova populations. Our results indicate a decrease in f_{WD} from 75% to 25%, accompanied by an increase in log(N/O) values. The observed trends are consistent with previous studies (Politano et al. 1995; José & Hernanz 1998). The right three panels in Figure 3 show the distribution of log (C/O) versus He/H for nova populations. Similar to log(N/O)versus He/H, the peak of He/H is larger with $f_{\rm WD}$ increase. The main reason is that He/H increases in the nuclear reaction zone with f_{WD} increase because of the ash of TNR mainly consisting of the element He, which leads to the increase of He/H in the nova ejecta.

Theoretically, it is very difficult to give the mixing factor. Using a one-dimensional (1D) Kolmogorov–Smirnov (K–S) test, we compare the simulated results with different f_{WD} to the observations via log(C/O), log(N/O) and log(Ne/O), as displayed in Figure 4. Although there are still large deviations, the results of the models with $f_{WD} = 25\%$ have a better agreement with the observations. It indicates that the mixing factor should be small. There are some observed novae which cannot be covered by our simulations. The main reasons are as follows: An asymmetric nova outburst also contributes to the discrepancies between theoretical results and observations. Mukai & Sokoloski (2019) suggested that the geometric distribution of nova ejecta is the shape of an equatorial torus, not symmetric. It indicates that ejecta from novae have very complicated structure. The code MESA is 1D, and it simulates nova eruptions as spherically symmetric events. Our model has its limitations. There are currently very few instances of twodimensional or three-dimensional simulations of nova eruptions. Therefore, we are unable to discuss the influence of asymmetric structures on our results. Observationally, there are very large observational errors for observing chemical

abundances. As shown in Figure 3, the observational errors can get up to ~ 5 . On observations, different authors provide different abundance values. Even for the same nova, there can be significantly different observational data. Therefore, the incompleteness of theoretical simulation and the large observational errors result in the discrepancy appearing in Figure 3.

Two upcoming recurrent novae, T Crb and M31N 1926-07c, are also shown in Figure 3. The former is expected to erupt again in 2024 (Zamanov et al. 2023), while the latter will do this in 2025 June (Shafter et al. 2022). Based on their WD masses, mass-accretion rates, and recurrence time, we have made an estimate for the abundance ratios of chemical elements for T Crb and M31N 1926-07c.

Compared to RGs or supernovae, nova ejecta have a negligible contribution to the ISM. However, observational evidence suggest that novae are the main source of oddnumbered nuclear elements ¹³C, ¹⁵N, and ¹⁷O (Livio & Truran 1994; Pavlenko et al. 2004). Figure 5 shows the distribution of isotopic abundance ratio for nova ejecta. The distributions of CNO isotopic abundance ratios in our simulations are cut into two regions. The right-upper regions mainly represent CO novae, while the left-bottom ones are from ONeMg novae. The observed estimate of $\log(^{12}C/^{13}C)$ is between \sim -0.5 (V2274 Cyg) and 0.7 (V705 Cas) (Banerjee & Ashok 2012; Das 2021). Our results are consistent with these observational estimates. Compared with RGs and the Sun, ¹²C/¹³C in nova ejecta is much lower. It means that nova outbursts produce a higher amount of ¹³C. However, ¹⁴N/¹⁵N and ¹⁶O/¹⁷O in ONeMg nova ejecta are lower than those of RGs, while they in CO nova ejecta are higher or closed. It indicates that ONeMg nova outbursts produce a higher amount of ¹⁵N and ¹⁷O.

3.4. Contribution of Chemical Abundances to the ISM

To calculate the contribution of chemical abundances to the ISM, we estimate the nova rate in the Galaxy. We assume that stars have been forming steadily over the course of 13.7 Gyr at the steady-state stellar production rate (Chomiuk & Povich 2011). In

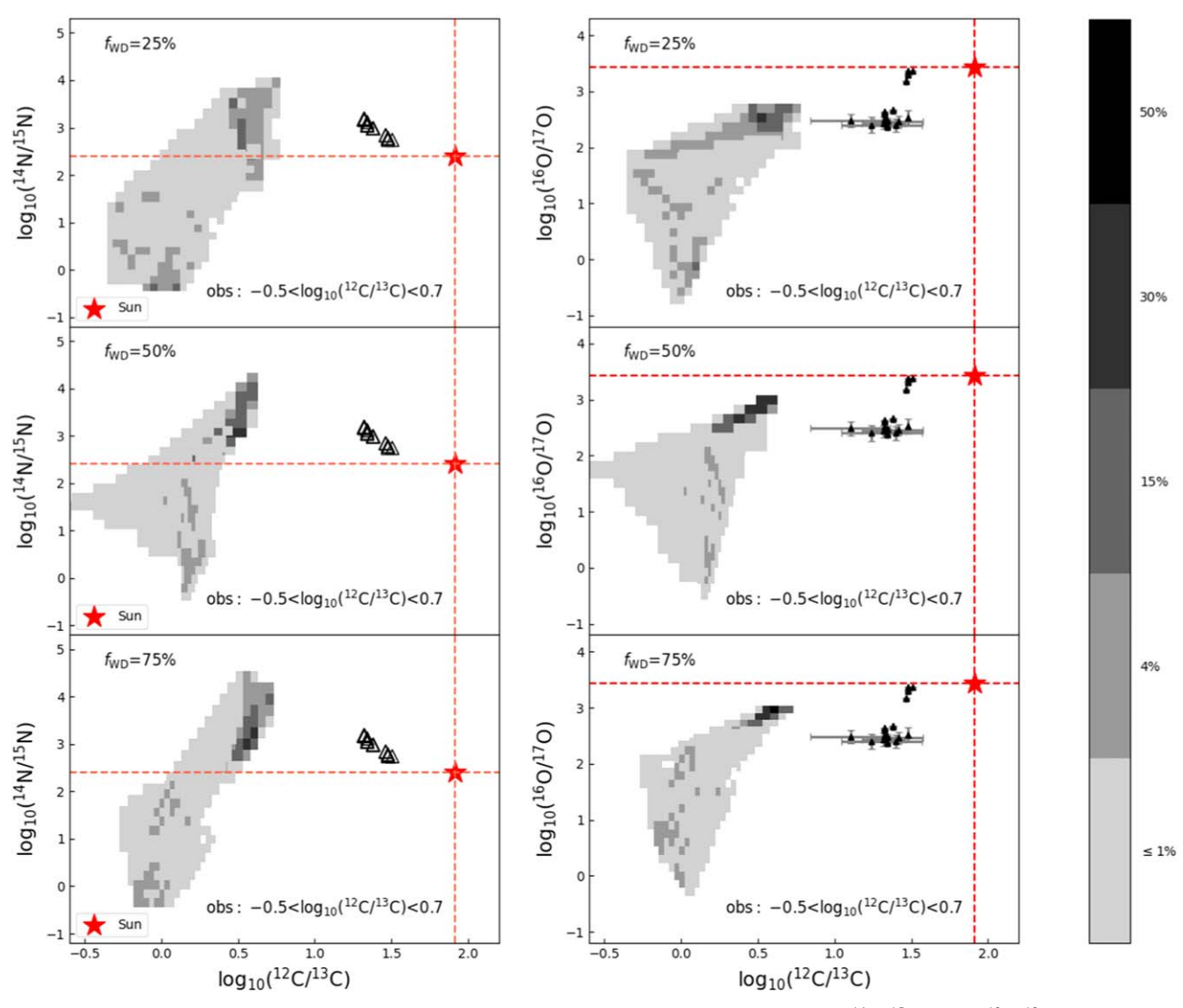


Figure 5. Distribution of CNO isotopic abundance ratios in nova ejecta. The left panels show the distribution of $\log^{14} N/^{15} N$) vs. $\log^{(12} C/^{13} C)$, while the right panels give the distribution of $\log^{(16} O/^{17} O)$ vs. $\log^{(12} C/^{13} C)$. We use the same normalization method as in Figure 3. The black hollow triangles and dots represent observed values from RGs (Smith & Lambert 1990; Halabi & Eid 2015), while the red pentagram represents the solar abundance (Anders & Grevesse 1989).

our model, a typical nova system can experience ~ 8000 eruptions, which is consistent with the value estimated by Bath & Shaviv (1978) and Molaro et al. (2020). If we assume that the birthrate of binaries with the primary higher than $0.8~M_{\odot}$ is 1.0 in the Galaxy (Han et al. 1995; Lü et al. 2006), the occurrence rate of nova outbursts is $\sim 130~\rm yr^{-1}$. In the observations, the nova occurrence rate in the Galaxy ranges from $\sim 20~\rm to~260~\rm yr^{-1}$ (Shafter 2002). Our estimate is within the scope provided by the observations. Tables $1-3~\rm give$ the annual contribution of some chemical elements from nova ejecta with different mixing degrees to the Galactic ISM.

Romano et al. (2017) investigated a chemical model of the Milky Way, and estimated that the average masses of 13 C, 15 N, and 17 O in a single eruption are $\sim 10^{-7}$, 10^{-7} , and $10^{-8} M_{\odot}$,

respectively. Our results are consistent with those in Romano et al. (2017). Considering the Galactic nova rate of 130 yr $^{-1}$, we can estimate that the average ejected mass of ^{13}C by novae is $8.0\times10^{-5}\,M_{\odot}\,\mathrm{yr}^{-1}\sim1.3\times10^{-4}\,M_{\odot}\,\mathrm{yr}^{-1}$, that of ^{15}N is $4.8\times10^{-6}\,M_{\odot}\,\mathrm{yr}^{-1}\sim2\times10^{-5}\,M_{\odot}\,\mathrm{yr}^{-1}$, and that of ^{17}O is $4.3\times10^{-6}\,M_{\odot}\,\mathrm{yr}^{-1}\sim1.7\times10^{-5}\,M_{\odot}\,\mathrm{yr}^{-1}$.

Asymptotic giant branch (AGB) stars have strong stellar wind, and also contribute to the enrichment of ISM chemistry. Theoretically, low-mass AGB stars have an insignificant contribution to the enrichment of odd-numbered nuclear elements (Iben 1975). However, the intermediate-mass AGB stars whose initial masses are higher than $\sim 3.5\,M_\odot$ can undergo hot bottom burning because the base of the convective envelope becomes hot enough, and can produce 13 C and 17 O

Ejecta Composition	Ejecta Mass $(M_{\odot} \text{ yr}^{-1})$		
•	CO Novae	ONeMg Novae	All Novae
¹ H	6.5×10^{-4}	1.3×10^{-4}	7.9×10^{-4}
⁴ He	3.9×10^{-4}	1.1×10^{-4}	5.0×10^{-4}
¹² C	2.2×10^{-4}	5.7×10^{-6}	2.2×10^{-4}
¹³ C	8.4×10^{-5}	3.6×10^{-6}	8.8×10^{-5}
¹⁴ N	3.9×10^{-4}	3.3×10^{-5}	4.2×10^{-4}
¹⁵ N	4.3×10^{-8}	1.8×10^{-5}	1.8×10^{-5}
¹⁶ O	6.3×10^{-4}	5.0×10^{-5}	6.8×10^{-4}
¹⁷ O	1.7×10^{-6}	5.4×10^{-6}	7.1×10^{-6}
²⁰ Ne	2.5×10^{-6}	6.7×10^{-5}	6.9×10^{-5}
²² Ne	1.1×10^{-5}	9.8×10^{-9}	1.1×10^{-5}

Ejecta Composition		Ejecta Mass $(M_{\odot} \text{ yr}^{-1})$		
J 1	CO Novae	ONeMg Novae	All Novae	
¹ H	4.7×10^{-4}	9.3×10^{-5}	5.6×10^{-4}	
⁴ He	2.9×10^{-4}	3.5×10^{-5}	3.3×10^{-4}	
¹² C	4.5×10^{-4}	4.2×10^{-5}	4.6×10^{-4}	
¹³ C	1.2×10^{-4}	1.2×10^{-5}	1.3×10^{-4}	
¹⁴ N	2.6×10^{-4}	1.2×10^{-5}	2.7×10^{-4}	
¹⁵ N	3.5×10^{-7}	1.9×10^{-5}	2.0×10^{-5}	
¹⁶ O	7.8×10^{-4}	9.1×10^{-5}	8.7×10^{-4}	
¹⁷ O	1.0×10^{-6}	1.6×10^{-5}	1.7×10^{-5}	
²⁰ Ne	2.2×10^{-6}	7.5×10^{-5}	7.7×10^{-5}	
²² Ne	1.6×10^{-5}	2.4×10^{-8}	1.6×10^{-5}	

via proton-capture nucleosynthesis (Iben 1975; Marigo 2001). Based on theoretical estimates, the contributions of AGB stars to ¹³C and ¹⁷O in the ISM are positive, but it is negative for ¹⁵N (Romano et al. 2017; Ventura et al. 2018). Marigo (2001) gave the detailed grid for chemical yields from low- and intermediate-mass stars. We can calculate the contribution of AGB stars to ¹³C, ¹⁵N and ¹⁷O by linear interpolation in Table 10 of Marigo (2001). Using the method of population synthesis, we create 10^6 binary systems, and $\sim 7\%$ of them can evolve into the systems including an AGB star whose mass is higher than $3.5\,M_\odot$. Each AGB star system can produce about $3\times10^{-4}\,M_\odot$ of $^{13}\mathrm{C},\ -1\times10^{-5}\,M_\odot$ of $^{15}\mathrm{N}$ and $4\times10^{-5}\,M_\odot$ of ¹⁷O. Then, the annual yields of ¹³C, ¹⁵N, and ¹⁷O produced by AGB stars are $\sim 2 \times 10^{-5} M_{\odot}$, $-7 \times 10^{-7} M_{\odot}$ and $3 \times 10^{-6} M_{\odot}$ respectively. The annual yields of ¹³C and ¹⁷O from nova ejection are $\sim 4-10$ and 1.5-5 times larger than those from AGB stars respectively. For ¹⁵N, the net yield from AGB stars is negative, which means that stars have a negative contribution to $^{15}{\rm N}$, while novae have a positive contribution $(4.8\times10^{-6}-2.0\times10^{-5}\,M_\odot\,{\rm yr}^{-1})$. In fact, the average abundances of ¹³C, ¹⁵N, and ¹⁷O of nova ejecta are about three orders of magnitude higher than those in the Sun. However, the average value of ¹⁴N/¹⁵N of nova ejecta is ~2.5 times higher than that in the Sun and about 1.5 times lower than that in a RG. It indicates that ¹⁵N may produced by additional production channels beyond novae (Muller et al. 2006). Pignatari et al. (2015) proposed that hydrogen ingestion into the helium shell of massive stars may account for the low ¹⁴N/¹⁵N. Therefore, we suggest that, compared to AGB stars, nova outbursts may be a more important source for the oddnumber nuclear elements ¹³C, ¹⁵N, and ¹⁷O in the Galactic ISM.

4. Conclusions

In order to investigate the contribution of nova eruptions to the Galactic ISM, we use MESA code to construct a detailed grid for novae including different WD masses, mass-accretion rates, and mixing degrees. With the population synthesis method, we create and evolve 10⁶ binary systems, and obtain about 2.5×10^4 nova systems. These nova systems evenly undergo ~8000 eruptions, and the Galactic nova rate is \sim 130 yr⁻¹. For a nova outburst, the range of ejecta masses is between $\sim 10^{-7}$ and $10^{-4} M_{\odot}$, and the average ejecta mass is about $10^{-5} M_{\odot}$. The mass ejected by novae into the Galactic ISM is even $\sim 10^{-3} M_{\odot} \text{ yr}^{-1}$. The average value of $^{12}\text{C}/^{13}\text{C}$ in nova ejecta is about an order magnitude lower than those on the surface of a RG, that for ¹⁶O/¹⁷O is about 5 times lower, and that for $^{14}N/^{15}N$ is about 1.5 times lower. The annual yields of 13 C and 17 O from nova ejection are \sim 4–10 and 1.5–5 times larger than those from AGB stars respectively. The average abundances of ¹³C, ¹⁵N, and ¹⁷O of nova ejecta are about three orders of magnitude higher than those in the Sun. Hence, the results indicate that in comparison with AGB stars, novae could be important contributors to the odd-number nuclear elements ¹³C, ¹⁵N and ¹⁷O found within the Galactic ISM.

Acknowledgments

This work received the generous support of the National Natural Science Foundation of China (NSFC, grant Nos. 12163005, U2031204, and 12373038), science research grants from the China Manned Space Project with No. CMSCSST-2021-A10, and the Natural Science Foundation of Xinjiang Nos. 2022D01D85 and 2022TSYCLJ0006.

Appendix Grid for Nova Models

We calculate the element yields of WD novae with different WD masses, mass-accretion rates and mixing degrees. The element yields of CO and ONeMg novae are given in Tables A1 and A2, respectively.

Table A1Element Yields for a Grid of CO Nova Models

$f_{\rm WD}$	М		$M_{ m CO~WD}(M_{\odot})$					
25%	$(M_{\odot} \text{ yr}^{-1})$	0.6	0.7	0.8	0.9	1.0	1.1	
¹ H	1×10^{-8}	5.96×10^{-1}	5.24×10^{-1}	5.27×10^{-1}	5.54×10^{-1}	5.52×10^{-1}	5.50×10^{-1}	
	1×10^{-9}	5.79×10^{-1}	5.26×10^{-1}	5.56×10^{-1}	5.18×10^{-1}	5.13×10^{-1}	4.24×10^{-1}	
	1×10^{-10}	5.29×10^{-1}	5.23×10^{-1}	5.58×10^{-1}	5.19×10^{-1}	5.16×10^{-1}	4.75×10^{-1}	
	1×10^{-11}	5.28×10^{-1}	5.14×10^{-1}	4.83×10^{-1}	4.05×10^{-1}	4.93×10^{-1}	4.57×10^{-1}	
⁴ He	1×10^{-8}	2.50×10^{-1}	2.10×10^{-1}	2.26×10^{-1}	2.33×10^{-1}	2.35×10^{-1}	2.34×10^{-1}	
	1×10^{-9}	2.40×10^{-1}	2.11×10^{-1}	2.37×10^{-1}	2.08×10^{-1}	2.11×10^{-1}	1.82×10^{-1}	
	1×10^{-10}	2.11×10^{-1}	2.10×10^{-1}	2.29×10^{-1}	2.08×10^{-1}	2.10×10^{-1}	2.31×10^{-1}	
	1×10^{-11}	2.19×10^{-1}	2.17×10^{-1}	2.40×10^{-1}	3.43×10^{-1}	2.28×10^{-1}	2.62×10^{-1}	
¹² C	1×10^{-8}	1.68×10^{-2}	5.30×10^{-2}	1.67×10^{-2}	1.60×10^{-2}	1.77×10^{-2}	1.75×10^{-2}	
	1×10^{-9}	1.29×10^{-2}	4.86×10^{-2}	8.00×10^{-3}	2.86×10^{-2}	1.79×10^{-2}	1.31×10^{-2}	
	1×10^{-10}	5.50×10^{-2}	4.38×10^{-2}	1.58×10^{-2}	2.76×10^{-2}	2.36×10^{-2}	1.73×10^{-2}	
	1×10^{-11}	2.43×10^{-2}	3.24×10^{-2}	8.52×10^{-3}	1.02×10^{-2}	1.25×10^{-2}	1.06×10^{-2}	
¹³ C	1×10^{-8}	2.78×10^{-3}	1.77×10^{-2}	6.17×10^{-3}	3.43×10^{-3}	4.04×10^{-3}	3.06×10^{-3}	
	1×10^{-9}	4.61×10^{-3}	2.26×10^{-2}	4.11×10^{-3}	3.22×10^{-2}	2.63×10^{-2}	9.22×10^{-2}	
	1×10^{-10}	1.90×10^{-2}	2.50×10^{-2}	9.12×10^{-3}	3.83×10^{-2}	3.45×10^{-2}	1.92×10^{-2}	
	1×10^{-11}	8.09×10^{-3}	7.60×10^{-3}	1.71×10^{-2}	2.22×10^{-2}	2.39×10^{-2}	2.41×10^{-2}	
¹⁴ N	1×10^{-8}	5.81×10^{-2}	6.42×10^{-2}	1.06×10^{-1}	9.06×10^{-2}	8.80×10^{-2}	9.10×10^{-2}	
	1×10^{-9}	7.49×10^{-2}	6.23×10^{-2}	9.48×10^{-2}	7.92×10^{-2}	9.83×10^{-2}	8.46×10^{-2}	
	1×10^{-10}	5.74×10^{-2}	6.69×10^{-2}	8.40×10^{-2}	7.34×10^{-2}	8.20×10^{-2}	8.35×10^{-2}	
	1×10^{-11}	1.00×10^{-1}	9.70×10^{-2}	1.16×10^{-1}	8.63×10^{-2}	8.56×10^{-2}	5.44×10^{-2}	
^{15}N	1×10^{-8}	4.93×10^{-6}	1.41×10^{-5}	2.52×10^{-5}	1.53×10^{-4}	2.61×10^{-4}	2.48×10^{-4}	
	1×10^{-9}	2.00×10^{-5}	9.65×10^{-5}	2.40×10^{-4}	5.54×10^{-4}	1.02×10^{-3}	1.61×10^{-2}	
	1×10^{-10}	4.42×10^{-5}	1.53×10^{-4}	2.64×10^{-4}	8.57×10^{-4}	1.57×10^{-3}	8.86×10^{-3}	
	1×10^{-11}	7.35×10^{-5}	1.35×10^{-4}	5.37×10^{-3}	1.75×10^{-2}	2.52×10^{-2}	6.33×10^{-2}	
¹⁶ O	1×10^{-8}	7.12×10^{-2}	1.26×10^{-1}	1.13×10^{-1}	9.77×10^{-2}	9.76×10^{-2}	9.85×10^{-2}	
	1×10^{-9}	8.36×10^{-2}	1.25×10^{-1}	9.40×10^{-2}	1.28×10^{-1}	1.27×10^{-1}	1.77×10^{-1}	
	1×10^{-10}	1.24×10^{-1}	1.26×10^{-1}	9.81×10^{-2}	1.28×10^{-1}	1.27×10^{-1}	1.28×10^{-1}	
	1×10^{-11}	1.20×10^{-1}	1.27×10^{-1}	1.24×10^{-1}	1.09×10^{-1}	1.23×10^{-1}	1.18×10^{-1}	
¹⁷ O	1×10^{-8}	1.32×10^{-4}	2.09×10^{-4}	3.03×10^{-4}	5.64×10^{-4}	6.14×10^{-4}	7.20×10^{-4}	
	1×10^{-9}	2.13×10^{-4}	3.20×10^{-4}	5.84×10^{-4}	9.27×10^{-4}	1.57×10^{-3}	5.12×10^{-3}	
	1×10^{-10}	2.30×10^{-4}	4.10×10^{-4}	4.74×10^{-4}	9.70×10^{-4}	1.50×10^{-3}	3.49×10^{-3}	
	1×10^{-11}	3.26×10^{-4}	7.40×10^{-4}	1.98×10^{-3}	3.03×10^{-3}	3.64×10^{-3}	6.09×10^{-3}	
²⁰ Ne	1×10^{-8}	2.64×10^{-3}	1.31×10^{-3}	1.60×10^{-3}	1.98×10^{-3}	1.97×10^{-3}	1.95×10^{-3}	
	1×10^{-9}	2.34×10^{-3}	1.35×10^{-3}	2.07×10^{-3}	1.26×10^{-3}	1.26×10^{-3}	1.45×10^{-3}	
	1×10^{-10}	1.36×10^{-3}	1.31×10^{-3}	1.98×10^{-3}	1.26×10^{-3}	1.26×10^{-3}	1.29×10^{-3}	
	1×10^{-11}	2.94×10^{-4}	1.13×10^{-5}	1.26×10^{-3}	1.53×10^{-3}	1.26×10^{-3}	1.26×10^{-3}	
²² Ne	1×10^{-8}	1.53×10^{-3}	2.57×10^{-3}	2.34×10^{-3}	2.05×10^{-3}	2.05×10^{-3}	2.07×10^{-3}	
	1×10^{-9}	1.76×10^{-3}	2.54×10^{-3}	1.98×10^{-3}	2.61×10^{-3}	2.61×10^{-3}	2.23×10^{-3}	
	1×10^{-10}	2.52×10^{-3}	2.57×10^{-3}	2.04×10^{-3}	2.61×10^{-3}	2.61×10^{-3}	2.54×10^{-3}	
	1×10^{-11}	2.38×10^{-5}	2.60×10^{-3}	2.60×10^{-3}	2.39×10^{-3}	2.61×10^{-3}	2.60×10^{-3}	
¹ H	1×10^{-8}	3.51×10^{-1}	3.52×10^{-1}	3.53×10^{-1}	4.55×10^{-1}	4.20×10^{-1}	3.27×10^{-1}	
	1×10^{-9}	3.50×10^{-1}	3.57×10^{-1}	4.36×10^{-1}	3.38×10^{-1}	3.34×10^{-1}	3.24×10^{-1}	
	1×10^{-10}	3.60×10^{-1}	3.50×10^{-1}	3.42×10^{-1}	3.42×10^{-1}	3.35×10^{-1}	3.24×10^{-1}	
	1×10^{-11}	3.40×10^{-1}	3.49×10^{-1}	4.25×10^{-1}	3.36×10^{-1}	3.81×10^{-1}	3.23×10^{-1}	
⁴ He	1×10^{-8}	1.47×10^{-1}	1.48×10^{-1}	1.56×10^{-1}	2.11×10^{-1}	1.95×10^{-1}	1.42×10^{-1}	
	1×10^{-9}	1.44×10^{-1}	1.52×10^{-1}	1.95×10^{-1}	1.38×10^{-1}	1.39×10^{-1}	1.41×10^{-1}	
	$1 \times 10^{-10} \\ 1 \times 10^{-11}$	$1.49 \times 10^{-1} \\ 1.39 \times 10^{-1}$	$1.46 \times 10^{-1} \\ 1.46 \times 10^{-1}$	$1.38 \times 10^{-1} \\ 1.80 \times 10^{-1}$	1.43×10^{-1} 1.38×10^{-1}	$1.43 \times 10^{-1} \\ 1.74 \times 10^{-1}$	1.41×10^{-1} 1.42×10^{-1}	
12								
¹² C	1×10^{-8}	1.35×10^{-1}	1.31×10^{-1}	1.00×10^{-1}	1.51×10^{-2}	2.46×10^{-2}	2.36×10^{-2}	

Table A1 (Continued)

f_{WD} \dot{M}				$M_{ m CO~V}$	$_{ m VD}(M_{\odot})$		
25%	$(M_{\odot} \text{ yr}^{-1})$	0.6	0.7	0.8	0.9	1.0	1.1
	1×10^{-9}	1.49×10^{-1}	1.40×10^{-1}	3.78×10^{-2}	1.15×10^{-1}	8.85×10^{-2}	2.98×10^{-2}
	1×10^{-10}	1.48×10^{-1}	1.41×10^{-1}	1.41×10^{-1}	1.00×10^{-1}	7.01×10^{-2}	3.07×10^{-2}
	1×10^{-11}	1.32×10^{-1}	1.24×10^{-1}	6.17×10^{-2}	9.72×10^{-2}	2.69×10^{-2}	3.33×10^{-2}
¹³ C	1×10^{-8}	3.17×10^{-2}	3.52×10^{-2}	2.89×10^{-2}	4.60×10^{-3}	9.64×10^{-3}	1.54×10^{-1}
	$1 \times 10^{-9} \\ 1 \times 10^{-10}$	$3.68 \times 10^{-2} \\ 3.90 \times 10^{-2}$	4.25×10^{-2} 4.93×10^{-2}	$1.81 \times 10^{-2} \\ 5.91 \times 10^{-2}$	7.01×10^{-2}	$7.38 \times 10^{-2} $ 9.02×10^{-2}	1.27×10^{-1} 1.22×10^{-1}
	1×10^{-11} 1×10^{-11}	3.90×10^{-2} 3.77×10^{-2}	4.93×10^{-2} 4.34×10^{-2}	3.53×10^{-2}	$7.56 \times 10^{-2} $ 7.48×10^{-2}	9.02×10^{-2} 1.87×10^{-2}	1.22×10^{-1} 1.02×10^{-1}
¹⁴ N	1×10^{-8}	8.82×10^{-2}	8.84×10^{-2}	1.23×10^{-1}	1.56×10^{-1}	1.67×10^{-1}	9.59×10^{-2}
IN	1×10^{-9} 1×10^{-9}	7.04×10^{-2}	6.54×10^{-2}	1.23×10^{-1} 1.35×10^{-1}	8.09×10^{-2}	1.07×10 1.08×10^{-1}	9.39×10^{-1} 1.15×10^{-1}
	1×10^{-10}	6.06×10^{-2}	6.46×10^{-2}	6.30×10^{-2}	8.67×10^{-2}	1.07×10^{-1}	1.20×10^{-1}
	1×10^{-11}	9.51×10^{-2}	9.02×10^{-2}	1.05×10^{-1}	9.61×10^{-2}	1.67×10^{-1}	1.39×10^{-1}
¹⁵ N	1×10^{-8}	4.16×10^{-6}	1.35×10^{-5}	1.03×10^{-5}	6.19×10^{-5}	2.01×10^{-4}	4.91×10^{-3}
	1×10^{-9}	1.44×10^{-5}	5.57×10^{-5}	2.52×10^{-4}	2.34×10^{-4}	3.80×10^{-4}	5.61×10^{-3}
	1×10^{-10}	3.43×10^{-5}	9.32×10^{-5}	1.43×10^{-4}	5.60×10^{-4}	1.17×10^{-3}	4.96×10^{-3}
	1×10^{-11}	6.61×10^{-5}	1.46×10^{-4}	3.74×10^{-4}	6.50×10^{-4}	2.00×10^{-3}	4.44×10^{-3}
¹⁶ O	1×10^{-8}	2.41×10^{-1}	2.39×10^{-1}	2.32×10^{-1}	1.52×10^{-1}	1.76×10^{-1}	2.47×10^{-1}
	1×10^{-9}	2.44×10^{-1}	2.36×10^{-1}	1.71×10^{-1}	2.50×10^{-1}	2.50×10^{-1}	2.46×10^{-1}
	1×10^{-10}	2.37×10^{-1}	2.43×10^{-1}	2.50×10^{-1}	2.45×10^{-1}	2.45×10^{-1}	2.46×10^{-1}
	1×10^{-11}	2.50×10^{-1}	2.42×10^{-1}	1.86×10^{-1}	2.50×10^{-1}	2.04×10^{-1}	2.46×10^{-1}
¹⁷ O	1×10^{-8}	2.01×10^{-4}	3.00×10^{-4}	3.08×10^{-4}	8.73×10^{-4}	1.15×10^{-3}	4.31×10^{-3}
	1×10^{-9}	2.59×10^{-4}	3.46×10^{-4}	6.45×10^{-4}	8.80×10^{-4}	1.35×10^{-3}	3.93×10^{-3}
	1×10^{-10}	2.53×10^{-4}	4.27×10^{-4}	5.63×10^{-4}	1.01×10^{-3}	1.66×10^{-3}	3.76×10^{-3}
	1×10^{-11}	2.84×10^{-4}	4.10×10^{-4}	5.97×10^{-4}	1.04×10^{-3}	1.90×10^{-3}	3.45×10^{-3}
²⁰ Ne	1×10^{-8}	9.73×10^{-4}	9.90×10^{-4}	1.08×10^{-3}	2.16×10^{-3}	1.83×10^{-3}	8.47×10^{-4}
	1×10^{-9}	9.30×10^{-4}	1.03×10^{-3}	1.91×10^{-3}	8.39×10^{-4}	8.39×10^{-4}	8.40×10^{-4}
	$\begin{array}{c} 1 \times 10^{-10} \\ 1 \times 10^{-11} \end{array}$	$1.02 \times 10^{-3} $ 1.58×10^{-5}	9.45×10^{-4} 9.52×10^{-4}	$8.39 \times 10^{-4} \\ 1.10 \times 10^{-3}$	9.01×10^{-4} 8.38×10^{-4}	8.93×10^{-4} 1.44×10^{-3}	8.39×10^{-4} 8.38×10^{-4}
²² Ne	1×10^{-8}	4.89×10^{-3}	4.86×10^{-3}	4.73×10^{-3}	3.18×10^{-3}	3.65×10^{-3}	5.05×10^{-3}
Ne	1×10^{-9} 1×10^{-9}	4.89×10^{-3} 4.95×10^{-3}	4.86×10^{-3} 4.79×10^{-3}	4.73×10^{-3} 3.54×10^{-3}	5.18×10^{-3} 5.07×10^{-3}	5.07×10^{-3}	5.05×10^{-3} 5.07×10^{-3}
	1×10 1×10^{-10}	4.93×10^{-3} 4.81×10^{-3}	4.79×10 4.92×10^{-3}	5.07×10^{-3}	4.98×10^{-3}	5.07×10^{-3} 5.00×10^{-3}	5.08×10^{-3}
	1×10^{-11} 1×10^{-11}	5.06×10^{-3}	4.91×10^{-3}	3.82×10^{-3}	5.07×10^{-3}	4.21×10^{-3}	5.07×10^{-3}
¹ H	1×10^{-8}	1.75×10^{-1}	1.92×10^{-1}	1.88×10^{-1}	2.98×10^{-1}	2.26×10^{-1}	1.47×10^{-1}
	1×10^{-9}	1.87×10^{-1}	2.06×10^{-1}	3.37×10^{-1}	1.63×10^{-1}	1.91×10^{-1}	1.44×10^{-1}
	1×10^{-10}	1.65×10^{-1}	1.92×10^{-1}	1.96×10^{-1}	1.78×10^{-1}	1.64×10^{-1}	2.20×10^{-1}
	1×10^{-11}	2.13×10^{-1}	1.93×10^{-1}	1.66×10^{-1}	2.73×10^{-1}	2.64×10^{-1}	2.46×10^{-1}
⁴ He	1×10^{-8}	1.06×10^{-1}	1.04×10^{-1}	1.03×10^{-1}	3.05×10^{-1}	1.89×10^{-1}	6.99×10^{-2}
	1×10^{-9}	1.03×10^{-1}	1.46×10^{-1}	1.59×10^{-1}	1.25×10^{-1}	1.95×10^{-1}	7.10×10^{-2}
	1×10^{-10}	1.40×10^{-1}	1.02×10^{-1}	9.98×10^{-2}	1.16×10^{-1}	7.85×10^{-2}	4.72×10^{-2}
	1×10^{-11}	1.40×10^{-1}	1.33×10^{-1}	8.22×10^{-2}	1.35×10^{-1}	1.26×10^{-1}	6.23×10^{-2}
¹² C	1×10^{-8}	1.49×10^{-1}	2.15×10^{-1}	1.81×10^{-1}	2.38×10^{-2}	1.14×10^{-1}	1.13×10^{-1}
	$1 \times 10^{-9} \\ 1 \times 10^{-10}$	$2.26 \times 10^{-1} \\ 2.34 \times 10^{-1}$	2.03×10^{-1} 2.22×10^{-1}	$1.07 \times 10^{-1} \\ 2.11 \times 10^{-1}$	$1.91 \times 10^{-1} \\ 1.65 \times 10^{-1}$	$1.39 \times 10^{-1} \\ 1.65 \times 10^{-1}$	1.00×10^{-1} 8.51×10^{-2}
	1×10^{-11} 1×10^{-11}	2.34×10^{-1} 1.89×10^{-1}	2.22×10^{-1} 1.93×10^{-1}	1.99×10^{-1}	7.52×10^{-2}	1.63×10^{-1} 1.03×10^{-1}	8.51×10^{-2} 6.64×10^{-2}
¹³ C	1×10^{-8}	4.26×10^{-2}	3.99×10^{-2}	3.66×10^{-2}	9.12×10^{-3}	3.65×10^{-2}	1.89×10^{-1}
C	1×10 1×10^{-9}	4.26×10 3.98×10^{-2}	3.99×10 4.65×10^{-2}	3.66×10 2.03×10^{-2}	9.12×10^{-2} 6.62×10^{-2}	3.65×10 4.65×10^{-2}	1.89×10 1.90×10^{-1}
	1×10 1×10^{-10}	4.84×10^{-2}	5.80×10^{-2}	5.83×10^{-2}	8.87×10^{-2}	1.13×10^{-1}	1.86×10^{-1}
	1×10^{-11}	4.43×10^{-2}	5.25×10^{-2}	7.26×10^{-2}	4.42×10^{-2}	1.01×10^{-1}	1.72×10^{-1}
¹⁴ N	1×10^{-8}	1.81×10^{-1}	1.03×10^{-1}	1.46×10^{-1}	1.83×10^{-1}	1.56×10^{-1}	9.79×10^{-2}
	1×10^{-9} 1×10^{-9}	9.50×10^{-2}	8.04×10^{-2}	1.30×10^{-1}	1.08×10^{-1}	1.24×10^{-1}	1.10×10^{-1}
	10	2.20 A 10	5.5 . A 10	1.00 // 10	1.00 // 10	1.2. // 10	1.10 / 10

Table A1 (Continued)

$f_{ m WD}$	M			$M_{ m CO~W}$	$_{ m VD}(M_{\odot})$		_
25%	$(M_{\odot} \text{ yr}^{-1})$	0.6	0.7	0.8	0.9	1.0	1.1
	$1 \times 10^{-10} \\ 1 \times 10^{-11}$	$7.00 \times 10^{-2} $ 9.60×10^{-2}	$7.76 \times 10^{-2} $ 9.73×10^{-2}	$8.77 \times 10^{-2} \\ 1.11 \times 10^{-1}$	1.07×10^{-1} 1.87×10^{-1}	$1.08 \times 10^{-1} \\ 1.07 \times 10^{-1}$	1.04×10^{-1} 1.17×10^{-1}
¹⁵ N	$ \begin{array}{c} 1 \times 10^{-8} \\ 1 \times 10^{-9} \\ 1 \times 10^{-10} \\ 1 \times 10^{-11} \end{array} $	5.15×10^{-6} 1.63×10^{-5} 3.61×10^{-5} 5.84×10^{-5}	1.45×10^{-5} 6.63×10^{-5} 9.69×10^{-5} 1.32×10^{-4}	8.57×10^{-6} 1.29×10^{-4} 8.64×10^{-5} 2.74×10^{-4}	5.29×10^{-5} 1.38×10^{-4} 5.25×10^{-4} 9.72×10^{-4}	1.06×10^{-4} 1.89×10^{-4} 7.07×10^{-4} 1.04×10^{-3}	2.11×10^{-3} 3.61×10^{-3} 4.69×10^{-3} 3.84×10^{-3}
¹⁶ O	$ \begin{array}{c} 1 \times 10^{-8} \\ 1 \times 10^{-9} \\ 1 \times 10^{-10} \\ 1 \times 10^{-11} \end{array} $	3.39×10^{-1} 3.41×10^{-1} 3.34×10^{-1} 3.09×10^{-1}	3.37×10^{-1} 3.10×10^{-1} 3.40×10^{-1} 3.22×10^{-1}	3.37×10^{-1} 2.38×10^{-1} 3.38×10^{-1} 3.60×10^{-1}	$ \begin{array}{c} 1.73 \times 10^{-1} \\ 3.39 \times 10^{-1} \\ 3.35 \times 10^{-1} \\ 2.77 \times 10^{-1} \end{array} $	2.69×10^{-1} 2.86×10^{-1} 3.61×10^{-1} 2.88×10^{-1}	3.70×10^{-1} 3.69×10^{-1} 3.41×10^{-1} 3.20×10^{-1}
¹⁷ O	$ \begin{array}{c} 1 \times 10^{-8} \\ 1 \times 10^{-9} \\ 1 \times 10^{-10} \\ 1 \times 10^{-11} \end{array} $	3.86×10^{-4} 2.46×10^{-4} 2.98×10^{-4} 2.91×10^{-4}	3.13×10^{-4} 3.38×10^{-4} 4.46×10^{-4} 4.10×10^{-4}	3.86×10^{-4} 4.97×10^{-4} 4.58×10^{-4} 6.97×10^{-4}	8.58×10^{-4} 7.56×10^{-4} 1.09×10^{-3} 9.84×10^{-4}	6.42×10^{-4} 8.02×10^{-4} 1.54×10^{-3} 1.56×10^{-3}	3.30×10^{-3} 3.69×10^{-3} 3.97×10^{-3} 3.74×10^{-3}
²⁰ Ne	$ \begin{array}{c} 1 \times 10^{-8} \\ 1 \times 10^{-9} \\ 1 \times 10^{-10} \\ 1 \times 10^{-11} \end{array} $	7.40×10^{-4} 7.25×10^{-4} 7.67×10^{-4} 1.04×10^{-3}	7.62×10^{-4} 1.01×10^{-3} 7.31×10^{-4} 8.97×10^{-4}	7.64×10^{-4} 1.79×10^{-3} 7.53×10^{-4} 5.36×10^{-4}	2.33×10^{-3} 7.07×10^{-4} 7.54×10^{-4} 1.39×10^{-3}	1.36×10^{-3} 1.18×10^{-3} 5.23×10^{-4} 1.26×10^{-3}	4.32×10^{-4} 4.20×10^{-4} 3.27×10^{-4} 4.19×10^{-4}
²² Ne	$ \begin{array}{c} 1 \times 10^{-8} \\ 1 \times 10^{-9} \\ 1 \times 10^{-10} \\ 1 \times 10^{-11} \end{array} $	6.92×10^{-3} 6.95×10^{-3} 6.84×10^{-3} 6.33×10^{-3}	6.88×10^{-3} 6.36×10^{-3} 6.93×10^{-3} 6.58×10^{-3}	6.87×10^{-3} 4.90×10^{-3} 6.89×10^{-3} 7.31×10^{-3}	3.81×10^{-3} 6.94×10^{-3} 6.86×10^{-3} 5.66×10^{-3}	5.66×10^{-3} 5.96×10^{-3} 7.34×10^{-3} 5.90×10^{-3}	7.49×10^{-3} 7.54×10^{-3} 6.54×10^{-3} 7.50×10^{-3}

Table A2
Element Yields for a Grid of ONeMg Nova Models

f_{WD}	М	$M_{ m ONe~WD}(M_{\odot})$				
25%	$(M_{\odot} \text{ yr}^{-1})$	1.1	1.2	1.3		
¹ H	1×10^{-8}	4.88×10^{-1}	5.07×10^{-1}	$4.57 \times 10^{-}$		
	1×10^{-9}	4.51×10^{-1}	4.88×10^{-1}	$4.51 \times 10^{-}$		
	1×10^{-10}	3.41×10^{-1}	2.98×10^{-1}	4.47×10^{-1}		
	1×10^{-11}	3.39×10^{-1}	4.84×10^{-1}	4.54×10^{-1}		
⁴ He	1×10^{-8}	2.59×10^{-1}	2.37×10^{-1}	$2.93 \times 10^{-}$		
	1×10^{-9}	3.11×10^{-1}	2.60×10^{-1}	$3.00 \times 10^{-}$		
	1×10^{-10}	1.87×10^{-1}	2.22×10^{-1}	3.00×10^{-1}		
	1×10^{-11}	1.85×10^{-1}	2.68×10^{-1}	$2.94 \times 10^{-}$		
¹² C	1×10^{-8}	3.09×10^{-3}	2.26×10^{-3}	7.93×10^{-3}		
	1×10^{-9}	5.65×10^{-3}	6.98×10^{-3}	1.20×10^{-2}		
	1×10^{-10}	4.88×10^{-3}	9.15×10^{-3}	1.16×10^{-2}		
	1×10^{-11}	4.03×10^{-3}	6.67×10^{-3}	7.88×10^{-3}		
¹³ C	1×10^{-8}	2.40×10^{-3}	1.36×10^{-3}	3.94×10^{-3}		
	1×10^{-9}	4.49×10^{-3}	4.03×10^{-3}	7.22×10^{-3}		
	1×10^{-10}	6.81×10^{-3}	1.35×10^{-2}	1.29×10^{-2}		
	1×10^{-11}	4.92×10^{-3}	6.99×10^{-3}	5.56×10^{-3}		
¹⁴ N	1×10^{-8}	1.57×10^{-2}	1.82×10^{-2}	1.88×10^{-2}		
	1×10^{-9}	1.31×10^{-2}	1.56×10^{-2}	2.23×10^{-2}		
	1×10^{-10}	1.09×10^{-2}	1.57×10^{-2}	2.55×10^{-2}		
	1×10^{-11}	9.62×10^{-3}	1.60×10^{-2}	2.45×10^{-2}		
¹⁵ N	1×10^{-8}	2.87×10^{-3}	7.24×10^{-4}	6.65×10^{-3}		
	$1 \times 10^{-9} \\ 1 \times 10^{-10}$	$1.30 \times 10^{-2} $ 2.67×10^{-2}	$1.28 \times 10^{-2} \\ 3.53 \times 10^{-2}$	2.59×10^{-2}		
	1×10^{-11} 1×10^{-11}	2.67×10^{-2} 2.75×10^{-2}	3.68×10^{-2}	5.11×10^{-2} 6.06×10^{-2}		
16						
¹⁶ O	$\begin{array}{c} 1 \times 10^{-8} \\ 1 \times 10^{-9} \end{array}$	9.26×10^{-2}	1.03×10^{-1}	5.52×10^{-2}		
	1×10^{-10} 1×10^{-10}	$7.06 \times 10^{-2} $ 1.69×10^{-1}	$6.42 \times 10^{-2} $ 1.42×10^{-1}	2.47×10^{-2} 7.36×10^{-3}		
	1×10^{-11} 1×10^{-11}	1.09×10 1.71×10^{-1}	3.78×10^{-2}	7.36×10^{-3} 3.35×10^{-3}		
¹⁷ O	1×10^{-8}	3.40×10^{-3}	2.55×10^{-3}	2.71×10^{-3}		
O	1×10^{-9} 1×10^{-9}	6.62×10^{-3}	5.93×10^{-3}	5.75×10^{-3}		
	1×10^{-10} 1×10^{-10}	2.92×10^{-2}	3.36×10^{-2}	1.41×10^{-2}		
	1×10^{-11}	3.35×10^{-2}	2.17×10^{-2}	2.17×10^{-2}		
²⁰ Ne	1×10^{-8}	9.12×10^{-2}	9.12×10^{-2}	9.07×10^{-2}		
1.0	1×10^{-9}	8.52×10^{-2}	9.10×10^{-2}	8.58×10^{-2}		
	1×10^{-10}	1.68×10^{-1}	1.69×10^{-1}	7.80×10^{-2}		
	1×10^{-11}	1.69×10^{-1}	8.51×10^{-2}	7.06×10^{-2}		
²² Ne	1×10^{-8}	5.65×10^{-5}	1.62×10^{-4}	8.38×10^{-6}		
	1×10^{-9}	2.27×10^{-5}	1.21×10^{-5}	1.95×10^{-6}		
	1×10^{-10}	8.33×10^{-5}	7.30×10^{-5}	6.53×10^{-3}		
	1×10^{-11}	6.23×10^{-5}	7.10×10^{-6}	7.70×10^{-7}		
¹ H	1×10^{-8}	3.68×10^{-1}	2.96×10^{-1}	2.83×10^{-1}		
	1×10^{-9}	2.89×10^{-1}	2.72×10^{-1}	2.33×10^{-1}		
	1×10^{-10}	3.80×10^{-1}	2.86×10^{-1}	2.50×10^{-1}		
	1×10^{-11}	3.69×10^{-1}	2.39×10^{-1}	3.59×10^{-1}		
⁴ He	1×10^{-8}	2.00×10^{-1}	2.05×10^{-1}	2.22×10^{-1}		
	1×10^{-9}	2.14×10^{-1}	2.32×10^{-1}	2.74×10^{-1}		
	1×10^{-10}	2.24×10^{-1}	2.27×10^{-1}	2.91×10^{-1}		
	1×10^{-11}	2.18×10^{-1}	3.19×10^{-1}	2.31×10^{-1}		

 1×10^{-11}

 1×10^{-8}

¹²C

 2.18×10^{-1}

 3.15×10^{-3}

 3.19×10^{-1}

 3.99×10^{-3}

Table A2 (Continued)

f_{WD}	М		$M_{ m ONe~WD}(M_{\odot})$	
25%	$(M_{\odot} \text{ yr}^{-1})$	1.1	1.2	1.3
	1×10^{-9}	2.84×10^{-3}	3.36×10^{-3}	5.99×10^{-3}
	1×10^{-10}	4.93×10^{-3}	9.73×10^{-3}	2.96×10^{-2}
	1×10^{-11}	1.14×10^{-2}	1.70×10^{-2}	9.48×10^{-3}
¹³ C	1×10^{-8}	2.37×10^{-3}	3.99×10^{-3}	4.28×10^{-3}
	$1 \times 10^{-9} \\ 1 \times 10^{-10}$	$8.40 \times 10^{-4} $ 6.06×10^{-3}	$9.99 \times 10^{-4} $ 4.31×10^{-3}	1.88×10^{-3} 2.50×10^{-2}
	1×10^{-11} 1×10^{-11}	6.00×10^{-3}	1.18×10^{-2}	6.78×10^{-3}
¹⁴ N	1×10^{-8}	2.27×10^{-2}	4.57×10^{-2}	2.48×10^{-2}
	1×10^{-9}	7.50×10^{-2}	8.62×10^{-2}	1.19×10^{-1}
	1×10^{-10}	9.18×10^{-2}	8.75×10^{-2}	9.47×10^{-2}
	1×10^{-11}	8.75×10^{-2}	7.67×10^{-2}	3.66×10^{-2}
¹⁵ N	1×10^{-8}	2.19×10^{-3}	7.49×10^{-4}	4.86×10^{-3}
	1×10^{-9}	1.19×10^{-2}	9.18×10^{-3}	2.16×10^{-2}
	$1 \times 10^{-10} \\ 1 \times 10^{-11}$	$1.57 \times 10^{-1} \\ 3.94 \times 10^{-2}$	3.53×10^{-2} 4.03×10^{-2}	6.82×10^{-2} 1.12×10^{-1}
¹⁶ O	$\begin{array}{c} 1 \times 10^{-8} \\ 1 \times 10^{-9} \end{array}$	1.77×10^{-1} 1.75×10^{-1}	$1.97 \times 10^{-1} \\ 1.62 \times 10^{-1}$	1.65×10^{-1}
	1×10^{-10} 1×10^{-10}	1.75×10^{-1} 1.34×10^{-1}	1.62×10^{-1} 1.42×10^{-1}	1.19×10^{-1} 6.17×10^{-2}
	1×10^{-11} 1×10^{-11}	1.34×10^{-1} 1.37×10^{-1}	1.06×10^{-1}	1.57×10^{-2}
¹⁷ O	1×10^{-8}	5.53×10^{-3}	4.53×10^{-3}	6.45×10^{-3}
U	1×10^{-9} 1×10^{-9}	1.43×10^{-3}	1.55×10^{-3}	0.43×10^{-3} 2.38×10^{-3}
	1×10^{-10}	4.24×10^{-3}	6.86×10^{-3}	1.31×10^{-2}
	1×10^{-11}	7.02×10^{-3}	1.11×10^{-2}	6.21×10^{-2}
²⁰ Ne	1×10^{-8}	1.58×10^{-1}	1.81×10^{-1}	1.79×10^{-1}
	1×10^{-9}	1.80×10^{-1}	1.79×10^{-1}	1.73×10^{-1}
	$1 \times 10^{-10} \\ 1 \times 10^{-11}$	$1.48 \times 10^{-1} \\ 1.58 \times 10^{-1}$	$1.75 \times 10^{-1} \\ 1.56 \times 10^{-1}$	1.57×10^{-1} 1.32×10^{-1}
²² Ne	1×10^{-8}	6.73×10^{-5}	2.85×10^{-4}	9.66×10^{-5}
Ne	1×10^{-9} 1×10^{-9}	5.17×10^{-5}	3.52×10^{-5}	9.00×10^{-5} 2.01×10^{-5}
	1×10^{-10} 1×10^{-10}	2.05×10^{-5}	4.03×10^{-5}	2.57×10^{-6}
	1×10^{-11}	1.12×10^{-5}	1.87×10^{-5}	8.15×10^{-7}
¹ H	1×10^{-8}	2.17×10^{-1}	1.27×10^{-1}	1.87×10^{-1}
	1×10^{-9}	1.81×10^{-1}	1.33×10^{-1}	1.06×10^{-1}
	1×10^{-10}	2.32×10^{-1}	2.17×10^{-1}	2.30×10^{-1}
	1×10^{-11}	2.70×10^{-1}	2.67×10^{-1}	4.46×10^{-1}
⁴ He	1×10^{-8}	1.37×10^{-1}	1.29×10^{-1}	1.71×10^{-1}
	1×10^{-9}	1.34×10^{-1}	1.20×10^{-1}	1.46×10^{-1}
	$1 \times 10^{-10} \\ 1 \times 10^{-11}$	$5.40 \times 10^{-2} $ 1.33×10^{-1}	8.14×10^{-2} 1.36×10^{-1}	1.94×10^{-1} 1.96×10^{-1}
¹² C	1×10^{-8}	4.02×10^{-3}	4.95×10^{-3}	9.59×10^{-3}
C	1×10^{-9} 1×10^{-9}	6.55×10^{-3}	4.93×10^{-3} 8.64×10^{-3}	9.39×10^{-2} 1.47×10^{-2}
	1×10^{-10}	5.63×10^{-3}	1.03×10^{-2}	2.43×10^{-2}
	1×10^{-11}	9.67×10^{-3}	8.41×10^{-3}	1.72×10^{-2}
¹³ C	1×10^{-8}	2.41×10^{-3}	3.82×10^{-3}	4.26×10^{-3}
	1×10^{-9}	3.65×10^{-3}	4.03×10^{-3}	4.98×10^{-3}
	1×10^{-10}	8.38×10^{-3}	6.29×10^{-3}	1.64×10^{-2}
	1×10^{-11}	1.47×10^{-2}	1.06×10^{-2}	1.49×10^{-2}
¹⁴ N	1×10^{-8}	2.59×10^{-2}	5.21×10^{-2}	2.96×10^{-2}
	1×10^{-9}	1.55×10^{-2}	1.95×10^{-2}	1.70×10^{-2}

 2.31×10^{-1}

 9.92×10^{-3}

Table A2 (Continued)

$f_{ m WD}$	M		$M_{ m ONe~WD}(M_{\odot})$	
25%	$(M_{\odot} \text{ yr}^{-1})$	1.1	1.2	1.3
	$1 \times 10^{-10} \\ 1 \times 10^{-11}$	1.03×10^{-2} 1.97×10^{-2}	$1.59 \times 10^{-2} $ 2.23×10^{-2}	3.85×10^{-2} 5.63×10^{-2}
¹⁵ N	$ \begin{array}{c} 1 \times 10^{-8} \\ 1 \times 10^{-9} \\ 1 \times 10^{-10} \\ 1 \times 10^{-11} \end{array} $	1.47×10^{-3} 8.44×10^{-3} 2.23×10^{-2} 4.21×10^{-2}	5.45×10^{-4} 5.63×10^{-3} 2.31×10^{-2} 6.90×10^{-2}	2.88×10^{-3} 1.37×10^{-2} 6.24×10^{-2} 1.57×10^{-1}
¹⁶ O	$ \begin{array}{c} 1 \times 10^{-8} \\ 1 \times 10^{-9} \\ 1 \times 10^{-10} \\ 1 \times 10^{-11} \end{array} $	2.84×10^{-1} 2.86×10^{-1} 2.88×10^{-1} 2.36×10^{-1}	3.14×10^{-1} 3.07×10^{-1} 2.57×10^{-1} 1.85×10^{-1}	2.44×10^{-1} 2.70×10^{-1} 1.33×10^{-1} 3.23×10^{-2}
¹⁷ O	$ \begin{array}{c} 1 \times 10^{-8} \\ 1 \times 10^{-9} \\ 1 \times 10^{-10} \\ 1 \times 10^{-11} \end{array} $	7.39×10^{-3} 1.46×10^{-2} 3.31×10^{-2} 4.13×10^{-2}	7.60×10^{-3} 1.26×10^{-2} 3.10×10^{-2} 6.70×10^{-2}	7.97×10^{-3} 2.19×10^{-2} 3.27×10^{-2} 7.60×10^{-2}
²⁰ Ne	$ \begin{array}{c} 1 \times 10^{-8} \\ 1 \times 10^{-9} \\ 1 \times 10^{-10} \\ 1 \times 10^{-11} \end{array} $	2.31×10^{-1} 2.42×10^{-1} 2.47×10^{-1} 2.25×10^{-1}	2.70×10^{-1} 2.64×10^{-1} 2.42×10^{-1} 2.21×10^{-1}	2.32×10^{-1} 2.54×10^{-1} 2.15×10^{-1} 2.17×10^{-1}
²² Ne	$ \begin{array}{c} 1 \times 10^{-8} \\ 1 \times 10^{-9} \\ 1 \times 10^{-10} \\ 1 \times 10^{-11} \end{array} $	4.15×10^{-4} 2.76×10^{-4} 3.08×10^{-4} 6.65×10^{-5}	4.70×10^{-4} 4.73×10^{-4} 1.86×10^{-4} 3.37×10^{-5}	1.33×10^{-4} 4.50×10^{-4} 6.56×10^{-5} 3.29×10^{-5}

```
References
Anders, E., & Grevesse, N. 1989, GeCoA, 53, 197
Banerjee, D. P. K., & Ashok, N. M. 2012, BASI, 40, 243
Bath, G. T., & Shaviv, G. 1978, MNRAS, 183, 515
Bennett, M. B., Wrede, C., Chipps, K. A., et al. 2013, PhRvL, 111, 232503
Chandrasekhar, S. 1931, ApJ, 74, 81
Chandrasekhar, S. 1935, MNRAS, 95, 207
Chen, H.-L., Woods, T. E., Yungelson, L. R., Gilfanov, M., & Han, Z. 2016,
        AS, 458, 2916
Chen, H.-L., Woods, T. E., Yungelson, L. R., et al. 2019, MNRAS, 490, 1678
Chen, X., Liu, Z., & Han, Z. 2024, PrPNP, 134, 104083
Chomiuk, L., Metzger, B. D., & Shen, K. J. 2021, ARA&A, 59, 391
Chomiuk, L., & Povich, M. S. 2011, AJ, 142, 197
Das, R. 2021, JApA, 42, 13
Denissenkov, P. A., Herwig, F., Bildsten, L., & Paxton, B. 2013, ApJ, 762, 8
Downen, L. N., Iliadis, C., José, J., & Starrfield, S. 2013, ApJ, 762, 105
Eggleton, P. P., Fitchett, M. J., & Tout, C. A. 1989, ApJ, 347, 998
Evans, A., Callus, C. M., Albinson, J. S., et al. 1988, MNRAS, 234, 755
Gao, J., Zhu, C., Lü, G., et al. 2024, ApJ, 971, 4
Gao, J., Zhu, C., Yu, J., et al. 2022, A&A, 668, A126
Ge, H., Hjellming, M. S., Webbink, R. F., Chen, X., & Han, Z. 2010, ApJ,
  717, 724
Ge, H., Webbink, R. F., Chen, X., & Han, Z. 2015, ApJ, 812, 40
Ge, H., Webbink, R. F., Chen, X., & Han, Z. 2020, ApJ, 899, 132
Gehrz, R. D., Truran, J. W., Williams, R. E., & Starrfield, S. 1998, PASP,
Guo, Y., Wu, C., & Wang, B. 2022, A&A, 660, A53
Hachisu, I., & Kato, M. 2015, ApJ, 798, 76
Hachisu, I., & Kato, M. 2019, ApJS, 242, 18
Halabi, G. M., & Eid, M. E. 2015, MNRAS, 451, 2957
Han, Z., Eggleton, P. P., Podsiadlowski, P., & Tout, C. A. 1995, MNRAS,
   277, 1443
```

```
Hassall, B. J. M., Snijders, M. A. J., Harris, A. W., et al. 1990, IAU Coll. 122:
   Physics of Classical Novae, Vol. 369, ed. A. Cassatella & R. Viotti
   (Berlin: Springer), 202
Hernanz, M. 2012, BASI, 40, 377
Hillman, Y., Prialnik, D., Kovetz, A., Shara, M. M., & Neill, J. D. 2014,
   MNRAS, 437, 1962
Horne, K., Welsh, W. F., & Wade, R. A. 1993, ApJ, 410, 357
Hurley, J. R., Tout, C. A., & Pols, O. R. 2002, MNRAS, 329, 897
Iben, I. J. 1975, ApJ, 196, 525
Iijima, T. 2006, A&A, 451, 563
José, J., & Hernanz, M. 1998, ApJ, 494, 680
José, J., & Hernanz, M. 2007, JPhG, 34, R431
José, J., Hernanz, M., & Coc, A. 1997, ApJL, 479, L55
José, J., Hernanz, M., & Iliadis, C. 2006, NuPhA, 777, 550
Kato, M., & Hachisu, I. 2009, ApJ, 699, 1293
Kato, M., & Hachisu, I. 2011, ApJ, 743, 157
Kennedy, C. R. 2011, PhD thesis, Michigan State University
Kovetz, A., & Prialnik, D. 1997, ApJ, 477, 356
Li, F., Zhu, C., Lü, G., & Wang, Z. 2016, PASJ, 68, 39
Livio, M., Shankar, A., & Truran, J. W. 1988, ApJ, 330, 264
Livio, M., & Truran, J. W. 1994, ApJ, 425, 797
Lodders, K., & Palme, H. 2009, M&PSA, 72, 5154
Lü, G., Yungelson, L., & Han, Z. 2006, MNRAS, 372, 1389
Lü, G., Zhu, C., Han, Z., & Wang, Z. 2008, ApJ, 683, 990
Lü, G., Zhu, C., & Podsiadlowski, P. 2013, ApJ, 768, 193
Lyke, J. E., Koenig, X. P., Barlow, M. J., et al. 2003, AJ, 126, 993
Marigo, P. 2001, A&A, 370, 194
Miller, G. E., & Scalo, J. M. 1979, ApJS, 41, 513
Molaro, P., Izzo, L., Bonifacio, P., et al. 2020, MNRAS, 492, 4975
Mukai, K., & Sokoloski, J. L. 2019, PhT, 72, 38
Muller, S., Guélin, M., Dumke, M., Lucas, R., & Combes, F. 2006, A&A,
  458, 417
Pavlenko, Y. V., Geballe, T. R., Evans, A., et al. 2004, A&A, 417, L39
Pavlenko, Y. V., Woodward, C. E., Rushton, M. T., Kaminsky, B., &
   Evans, A. 2010, MNRAS, 404, 206
Paxton, B., Bildsten, L., Dotter, A., et al. 2011, ApJS, 192, 3
Paxton, B., Cantiello, M., Arras, P., et al. 2013, ApJS, 208, 4
Paxton, B., Marchant, P., Schwab, J., et al. 2015, ApJS, 220, 15
Pignatari, M., Zinner, E., Hoppe, P., et al. 2015, ApJL, 808, L43
Politano, M., Starrfield, S., Truran, J. W., Weiss, A., & Sparks, W. M. 1995,
    pJ, 448, 807
Prialnik, D. 1986, ApJ, 310, 222
Ritossa, C., Garcia-Berro, E., & Iben, I. J. 1996, ApJ, 460, 489
Romano, D., Matteucci, F., Zhang, Z. Y., Papadopoulos, P. P., & Ivison, R. J.
  2017, MNRAS, 470, 401
Saizar, P., Starrfield, S., Ferland, G. J., et al. 1991, ApJ, 367, 310
Schaefer, B. E. 2022, MNRAS, 517, 3640
Schreiber, M. R., Zorotovic, M., & Wijnen, T. P. G. 2016, MNRAS,
Schwartzman, E., Kovetz, A., & Prialnik, D. 1994, MNRAS, 269, 323
Schwarz, G. J., Shore, S. N., Starrfield, S., & Vanlandingham, K. M. 2007a,
   ApJ, 657, 453
Schwarz, G. J., Woodward, C. E., Bode, M. F., et al. 2007b, AJ, 134, 516
Selvelli, P., & Gilmozzi, R. 2019, A&A, 622, A186
Shafter, A. W. 2002, in AIP Conf. Ser. 637, Classical Nova Explosions, ed.
   M. Hernanz & J. José (Melville, NY: AIP), 462
Shafter, A. W., Hornoch, K., Kučáková, H., et al. 2022, RNAAS, 6, 214
Shara, M. M., Livio, M., Moffat, A. F. J., & Orio, M. 1986, ApJ, 311, 163
Shara, M. M., Prialnik, D., Hillman, Y., & Kovetz, A. 2018, ApJ, 860, 110
Shen, K. J., & Quataert, E. 2022, ApJ, 938, 31
Shore, S. N., Schwarz, G., Bond, H. E., et al. 2003, AJ, 125, 1507
Smith, D. A., Dhillon, V. S., & Marsh, T. R. 1998, MNRAS, 296, 465
Smith, V. V., & Lambert, D. L. 1990, ApJS, 72, 387
Starrfield, S., Bose, M., Iliadis, C., et al. 2020, ApJ, 895, 70
Starrfield, S., Gehrz, R. D., & Truran, J. W. 1997, in AIP Conf. Ser. 402,
   Astrophysical Implications of the Laboratory Study of Presolar Materials,
   ed. T. J. Bernatowicz & E. Zinner (Melville, NY: AIP), 203
Starrfield, S., Truran, J. W., Sparks, W. M., & Kutter, G. S. 1972, ApJ,
```

Han, Z.-W., Ge, H.-W., Chen, X.-F., & Chen, H.-L. 2020, RAA, 20, 161

Thoroughgood, T. D., Dhillon, V. S., Littlefair, S. P., Marsh, T. R., & Smith, D. A. 2001, MNRAS, 327, 1323

Tylenda, R., Kamiński, T., & Mehner, A. 2019, A&A, 628, A124

Vanlandingham, K. M., Schwarz, G. J., Shore, S. N., Starrfield, S., & Wagner, R. M. 2005, ApJ, 624, 914

Ventura, P., Karakas, A., Dell'Agli, F., García-Hernández, D. A., & Guzman-Ramirez, L. 2018, MNRAS, 475, 2282

Yaron, O., Prialnik, D., Shara, M. M., & Kovetz, A. 2005, ApJ, 623, 398

Zamanov, R., Boeva, S., Latev, G. Y., et al. 2023, A&A, 680, L18

Zhu, C.-H., Lü, G.-L., Lu, X.-Z., & He, J. 2023, RAA, 23, 025021